Dalton Transactions

ROYAL SOCIETY OF CHEMISTRY

PAPER

View Article Online
View Journal | View Issue

Cite this: *Dalton Trans.*, 2025, **54**, 1956

$Na_2B_{12}Si_6Se_{18}$: a novel B_{12}-cluster-containing quaternary selenoborate framework material†

Gopabandhu Panigrahi, Hunter B. Tisdale, Gregory Morrison and Hans-Conrad zur Loye *

Received 8th November 2024,
Accepted 3rd December 2024

DOI: 10.1039/d4dt03139c

rsc.li/dalton

We report the successful synthesis of the new quaternary, three-dimensional $Na_2Si_6B_{12}Se_{18}$ material using a solid-state synthesis route. This compound is characterized by a unique framework structure that features the rare icosahedral $[B_{12}]^{10+}$ cation which is connected *via* Si_2Se_6 polyhedral units into a 3D framework structure with Na^+ ions located inside the channels. The $Na_2Si_6B_{12}Se_{18}$ compound crystallizes in the cubic crystal system in the space group $Im\bar{3}$, with lattice parameter a = 11.91110(10) Å and unit cell volume of 1689.88(4) Å^3. The 3D framework of the $[Si_6B_{12}Se_{18}]^{2-}$ anion contains B_{12} icosahedra with six of their edges bridged by tetrahedral $SiSe_4$ groups. The B_{12} icosahedral units are connected by the $SiSe_4$ tetrahedral units which bridge between each B_{12} icosahedron. Ultraviolet–Visible (UV-vis) spectroscopy revealed that $Na_2Si_6B_{12}Se_{18}$ exhibits semiconducting behavior with an estimated bandgap of 2.1(1) eV. *In situ* powder X-ray diffraction (PXRD) studies were conducted to investigate the phase formation of this compound as a function of temperature to obtain information of its thermal stability and structural evolution.

Introduction

The linkage of SiQ_4 (Q = S, Se or Te) tetrahedra forms a wide variety of network structures, as observed in numerous thio- and selenosilicate compounds. These structures are not only intriguing from a structural perspective but also hold significant potential for various applications in materials science and technology. The synthesis of compounds that incorporate SiQ_4 units as bridges between B_{12} clusters is particularly fascinating and represents an area of great interest within the field of solid-state inorganic chemistry. Boron is often found in electron deficient compounds, most notably the boron hydrides, where the electron deficiency significantly influences the chemistry and leads to the formation of various intriguing cluster species.[1] One notable class of these clusters is the *closo*-borane anions ($B_{12}H_{12}^{2-}$), which are known for their remarkable chemical stability to both air and moisture.[2,3] This stability arises from the large energy gap between the highest occupied molecular orbital (HOMO) and the lowest unoccupied molecular orbital (LUMO), making these compounds less reactive under ambient conditions. In recent years, the synthesis of various thio- and selenoborates has advanced considerably due to modern synthetic techniques. These compounds, characterized by boron–chalcogen bonds, form the chalcoborate class of materials and exhibit diverse structural motifs. Typically, in these structures, the boron atom (B^{3+}) is found in either a trigonal or tetrahedral coordination environment.[4–7] Examples of non-oxide chalcoborates where B^{3+} is present in such coordination environments include the compounds $M_8[B_{12}(BSe_3)_6]$, $M_4Hg_2[B_{12}(BSe_3)_6]$, BaB_2Se_6, SrB_2S_4, $CsBSe_3$ and others.[8–13] These compounds highlight the versatility of boron-chalcogen bonding in forming complex structures. The structural motifs in binary, ternary, and quaternary boron chalcogenides often include units such as B_8Q_{16}, $(BQ_2)_n$, $(BQ_3)^{3-}$, and $(B_2Q_5)^{2-}$(Q = S or Se).[4–7,14] In some cases, as observed in compounds like $Li_9B_{19}S_{33}$ and $Li_{4-2x}Sr_{2+x}B_{10}S_{19}$ (where x = 0.27), the structure is defined by corner-sharing BS_4 tetrahedral units.[15] These examples illustrate the complexity and richness of boron-chalcogen chemistry, which continues to be an area of significant interest in materials science and inorganic chemistry.

Boron chalcogenides are not only expanding the landscape of structural chemistry but are also playing a pivotal role in guiding the discovery of new materials with significant potential for applications; for example, these compounds are at the forefront of research into high-performance IR birefringent materials, advanced nonlinear optical materials, and promising solid state electrolytes.[16–20]

In addition to the intriguing structures and properties of boron chalcogenides containing SiQ_4 tetrahedra and B_{12} clus-

Department of Chemistry and Biochemistry, University of South Carolina, Columbia, SC, 29208, USA. E-mail: zurloye@mailbox.sc.edu

†Electronic supplementary information (ESI) available: EDS tabulated data, PXRD patterns, and TGA plot. CCDC 2362801. For ESI and crystallographic data in CIF or other electronic format see DOI: https://doi.org/10.1039/d4dt03139c

ters, it is noteworthy that very few compounds have been reported in the quaternary systems involving these components. Through an extensive literature survey, we identified only one quaternary compound, $CrSi_3(B_{12})Se_{12}$, within the *M*–Si–B–*Q* (where *M* represents alkali, alkaline earth, or transition metals, and *Q* refers to S, Se, and Te) system.[21] This scarcity of reported compounds highlights the novelty and significance of our findings.

In this study, we report the synthesis of a new quaternary framework structure, $Na_2B_{12}Si_6Se_{18}$, within the *A*–B–Si–*Q* (A = alkali or alkaline earth metal) system, marking the first discovery in this series. We successfully synthesized both high-quality single crystals and phase-pure polycrystalline materials of $Na_2B_{12}Si_6Se_{18}$. The physical properties of this compound were investigated using various analytical techniques, including single crystal X-ray diffraction, powder X-ray diffraction, thermogravimetric analysis (TGA), differential scanning calorimetry (DSC), and UV-Vis spectroscopy. Moreover, we conducted a detailed *in situ* X-ray diffraction study of the formation of $Na_2B_{12}Si_6Se_{18}$ to gain a deeper understanding of the temperature dependence of its phase formation process from the precursor reactants. This comprehensive analysis not only provides insights into the synthesis conditions required for the formation of $Na_2B_{12}Si_6Se_{18}$, but also contributes valuable knowledge to the field of solid-state inorganic chemistry, potentially paving the way for the discovery of other novel quaternary compounds in this system.

Experimental section

Eu_2O_3 (99.9%, Alfa Aesar), selenium powder (99.999% Fisher scientific), U_3O_8 (International Bio-Analytical Industries, Inc.,), boron (crystalline 100 mesh, 99.9%, Beantown Chemicals), SiO_2 (amorphous powder, 99.9%, Alfa Aesar), NaCl (99.9%, Alfa Aesar) and $CaCl_2$ (99.9%, Alfa Aesar) were utilized. The NaCl–$CaCl_2$ eutectic mixture used for synthesis was stored in a drying oven set to 260 °C to maintain the anhydrous state of the salts.

Synthesis of EuSe

EuSe was synthesized by combining 600 mg of Eu_2O_3, 300 mg of Se, and 80 mg of B in a sealed, evacuated silica tube. The reactant mixture was subjected to heating at 900 °C for 24 hours, resulting in the formation of EuSe. This material served as a precursor for subsequent reactions.[22,23]

Single crystal synthesis of $Na_2B_{12}Si_6Se_{18}$

During an attempt to synthesize a pentanary compound with the target composition $CaEuUSi_2Se_8$, $Na_2B_{12}Si_6Se_{18}$ was unexpectedly obtained. The reaction yielded light yellow, transparent crystals along with black and red impurities (see Fig. S1 and S2†). The Scanning electron microscopy (SEM) image of this light yellow crystal and its Energy Dispersive X-ray Spectroscopy (EDS) plot are provided in the ESI file (Fig. S1, S2 and Table. S1†). Additional details about the optimization of the synthesis conditions can be found in the ESI.†

The optimized reaction conditions for crystal growth are: 50 mg of EuSe, 20 mg of boron (B), and 90 mg of selenium (Se), supplemented with 75 mg of a NaCl/$CaCl_2$ flux mixture was sealed in a carbon coated fused silica tube and heated to 800 °C over a period of 12 hours, held at this temperature for 48 hours, and then gradually cooled to 550 °C over a period of 48 hours. Under these conditions, the transparent $Na_2B_{12}Si_6Se_{18}$ crystals consistently form.

Synthesis of polycrystalline $Na_2B_{12}Si_6Se_{18}$ compound

To obtain a phase-pure $Na_2B_{12}Si_6Se_{18}$ sample, a stoichiometric mixture of Na_2Se, Si, B, and Se (in the molar ratio of 1 : 6 : 12 : 17) was prepared. This mixture was sealed in a carbon coated fused silica tube and heated to 800 °C over a period of 12 hours, dwelling at 800 °C for 48 hours, and then cooling to 550 °C over another 48 hours before allowing the tube to return to room temperature. This method successfully yielded phase-pure $Na_2B_{12}Si_6Se_{18}$. The EDS analyses of the polycrystalline $Na_2B_{12}Si_6Se_{18}$ samples are shown in Fig. S3, S4 and Table S2.†

Caution: *Boron selenides are prone to moisture sensitivity, leading to the generation of H_2Se gas upon contact with water or moisture. Therefore, all reaction procedures must be conducted within fume hoods, with strict adherence to safety protocols.*

Single crystal X-ray diffraction (SCXRD)

X-ray intensity data from a block shaped light yellow transparent crystal of $Na_2B_{12}Si_6Se_{18}$ were collected at 299(2) K using a Bruker D8 QUEST diffractometer equipped with a PHOTON-II area detector and an Incoatec microfocus source (Mo Kα radiation, λ = 0.71073 Å).[24] The detector to crystal distance of 40 mm was fixed, and an exposure time of 10 s per frame was used for the data collection. The raw area detector data frames were reduced and corrected for absorption effects using the SAINT+ and SADABS programs.[25] Final unit cell parameters were determined by least-squares refinement over a large number (>5500) of reflections taken from the data set. An initial structural model was obtained with SHELXT.[26] Subsequent difference Fourier calculations and full-matrix least-squares refinement against F^2 were performed with SHELXL-2018.[27]

The $Na_2B_{12}Si_6Se_{18}$ compound crystallizes in the space group $Im\bar{3}$ of the cubic crystal system. The asymmetric unit consists of two selenium, one silicon, one boron, and one sodium atomic positions. Se1 and B1 atoms are located on mirror planes (Wyckoff site 24*g*), Se2 and Si1 atoms are located on *mm*2.. planes (Wyckoff site 12*e* and 12*d*), and the Na present on .–3. symmetry (Wyckoff site 8*c*). The occupancy of the Na atom was determined to be 0.49 during free refinement of the crystal structure and subsequently fixed at 0.50 for charge balance. All atoms were refined with anisotropic displacement parameters. Crystallographic and refinement data pertinent to the title compound are provided in Table 1.

Table 1 Crystallographic data for $Na_2B_{12}Si_6Se_{18}$

Crystal data	
Chemical formula	$Na_2B_{12}Si_6Se_{18}$
Formula weight	1765.38
Crystal system, space group	Cubic, $Im\bar{3}$
Temperature (K)	299(2)
a (Å)	11.91110(10)
V (Å^3)	1689.88(4)
Z	2
Radiation type	Mo Kα
μ (mm^{-1})	19.66
Crystal size (mm)	0.31 × 0.06 × 0.03
T_{min}, T_{max}	0.353, 0.494
No. of measured, independent and observed [$I > 2\sigma(I)$] reflections	6350, 531, 477
R_{int}	0.028
$R[F^2 > 2\sigma(F^2)]$, w$R(F^2)$, S	0.020, 0.046, 1.08
$\Delta\rho_{max}$, $\Delta\rho_{min}$ (e Å^{-3})	1.53, −0.48

Powder X-ray diffraction (PXRD)

Powder X-ray diffraction (PXRD) data were obtained by analyzing finely ground powder samples of $Na_2B_{12}Si_6Se_{18}$ prepared from stoichiometric amounts of reactants in a solid state reaction. PXRD data were collected on a Bruker D2 PHASER diffractometer using Cu Kα radiation (λ = 1.5418 Å) over the 2θ range 5–65° with a step size of 0.02°. The observed reflections of the PXRD patterns were indexed based on the simulated PXRD patterns obtained from the single crystal data. Fig. 1.

Energy-dispersive X-ray spectroscopy (EDS)

EDS data were collected on single crystals by mounting them directly onto an SEM stub using conducting carbon tape. Quantitative elemental analysis was performed utilizing a Tescan Vega-3 SEM instrument fitted with a Thermo EDS attachment. The SEM was operated in a low-vacuum mode with a 15–20 kV accelerating voltage and a 40 second accumulation time. The summarized SEM results can be found in the ESI.†

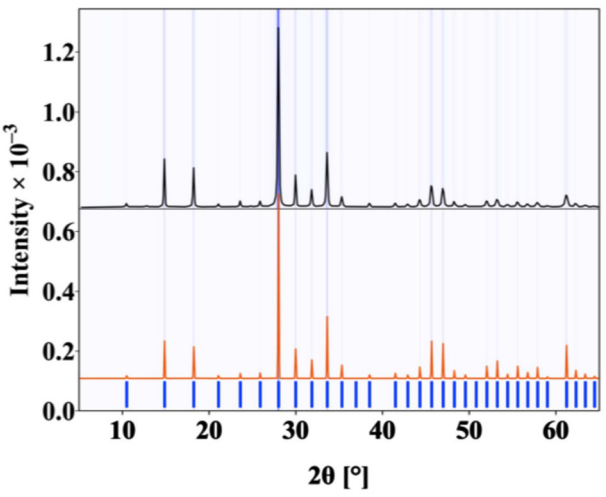

Fig. 1 The PXRD patterns of polycrystalline $Na_2B_{12}Si_6Se_{18}$ compound (simulated pattern (red), experimental pattern (black) and Bragg position (blue)).

UV-visible spectroscopy

UV-visible reflectance spectra were recorded using a PerkinElmer Lambda 35 UV-Vis spectrophotometer. The spectrophotometer was operated in the diffuse reflectance mode and was equipped with an integrating sphere. Reflectance data were converted internally to absorbance *via* the Kubelka–Munk function. Spectra were recorded over the 200 nm (6.2 eV)–900 nm (1.3 eV) range at room temperature and ambient condition on powder samples.[28]

Thermogravimetric analysis (TGA) and differential scanning calorimetry (DSC)

TGA/DSC data were collected on polycrystalline powder samples by utilizing a Texas Instruments SDT Q600 Simultaneous TGA/DSC. An alumina pan served as the sample holder. The samples were heated from room temperature to 500 °C at a rate of 5 °C min^{-1} under nitrogen gas with a controlled flow rate of 100 mL min^{-1}. Subsequently, the resulting powders were further analyzed by PXRD for phase identification.

In situ powder X-ray diffraction (PXRD)

In situ PXRD measurements were conducted using a Rigaku SmartLab equipped with a 9 kW rotating Mo Kα anode utilizing cross-beam optics (convergent radiation), an Anton Paar HTK1200N high-temperature oven chamber, and a capillary rotation attachment. A mixture of Na_2Se, Si, B, and Se (in the molar ratio of 1 : 6 : 12 : 17), the same as used to prepare phase-pure powders of $Na_2B_{12}Si_6Se_{18}$ as described above, was loaded into quartz capillary (OD = 1 mm, ID = 0.9 mm) that was previously sealed at one end using a MAPP/oxygen mixture torch. Once partially filled with the reaction mixture, the capillary was sealed using clay. The capillary was placed into the capillary rotation attachment which was then loaded into the HTK1200N. Once the capillary was set to rotate and the X-ray beam was aligned with the precise height of capillary, the capillary was heated to 800 °C at 5 °C min^{-1} with 30 min PXRD measurements from 4.5–35° 2θ taken at 50 °C increments until 600 °C and then at 20 °C increments up to 800 °C. Then, the capillary was held at 800 °C and 10 sequential PXRD measurements were taken, again 30 min in length from 4.5–35° 2θ. Finally, the capillary was cooled to 50 °C at 5 °C min^{-1} with 30 min PXRD measurements from 4.5–35° 2θ taken at 50 °C increments.

Results and discussion

Structure of the framework

The X-ray structure determination revealed that the compound consists of a complex three-dimensional framework with tunnels containing Na-ions (Fig. 2a and b). This framework is constructed from interconnected $SiSe_4$ tetrahedra and B_{12} ico-

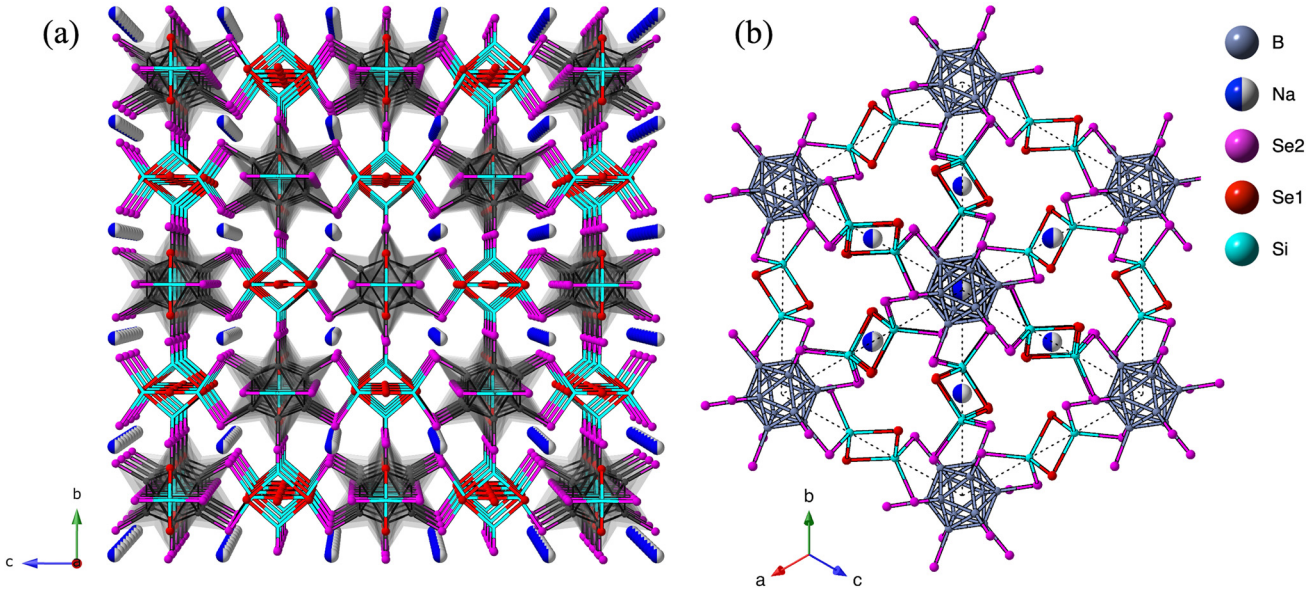

Fig. 2 The unit cell representation of $Na_2B_{12}Si_6Se_{18}$ (a) along a-axis, and (b) along [111] direction.

sahedra, with an overall composition of $Na_2B_{12}Si_6Se_{18}$. Chalcogenides containing B_{12} icosahedra, aside from halogenides or hydroxides, are relatively rare.[22,29,30] The observed B_{12} icosahedron is connected to twelve Se atoms, a structural motif that has been identified in only a few other recently reported compounds, such as $CrSi_3(B_{12})Se_{12}$, $A_8[B_{12}(BSe_3)_6]$, and $Sn_{4-\delta}B_{12}Se_{12}[Q_x]$ (where Q = Se, Te).[9,21,31] The structure of $Na_2B_{12}Si_6Se_{18}$ shows similarities to other quaternary compounds, such as $Sn_{4-\delta}B_{12}Se_{12}[Q_x]$ and $CrSi_3(B_{12})Se_{12}$, both of which also exhibit three-dimensional frameworks that incorporate B_{12} icosahedral clusters. In the $Sn_{4-\delta}B_{12}Se_{12}[Q_x]$ composition, the 3D framework is built from $(B_{12}Se_{12})^{14-}$ anionic *closo*-borane clusters that are connected along the *c*-axis by octahedral Sn^{2+} centers. These octahedral units form infinite parallel $[SnB_{12}Se_{12}]^{12-}$ columns that accommodate chains of neutral chalcogen atoms within the tunnels. Similarly, the $CrSi_3(B_{12})Se_{12}$ compound forms a 3D structure comprising $SiSe_4$ tetrahedra, $CrSe_6$ octahedra, and B_{12} icosahedra. In this structure, the tunnels formed by the 3D framework are filled with disordered Se atoms. The structural similarities between $Na_2B_{12}Si_6Se_{18}$ and these quaternary chalcogenides highlight a common motif of B_{12} icosahedral clusters linked by various metal centers, forming three-dimensional networks that can accommodate guest ions or atoms within the tunnels. This feature could potentially influence the physical properties, such as ion conductivity or electronic behavior, making these compounds of particular interest for further study.

In the quaternary composition $Na_2B_{12}Si_6Se_{18}$, the three-dimensional (3D) anionic framework, denoted as $[B_{12}Si_6Se_{18}]^{2-}$, is formed by the connection of $[B_{12}Se_{12}]^{14-}$ icosahedra with Si_2Se_6 tetrahedral units. The $[B_{12}Se_{12}]^{14-}$ cluster is a central feature of this framework, where the Se1 atoms act as bridging elements between the B_{12} icosahedral cluster and the $SiSe_4$ tetrahedra. The structure is further stabilized as the $B_{12}Se_{12}$ units share six of their edges with adjacent $SiSe_4$ tetrahedra, creating a robust and interconnected network. Within the $SiSe_4$ tetrahedra, two distinct types of selenium atoms, Se1 and Se2, play crucial roles in the framework's architecture. Se1 serves as a bridge, connecting the $SiSe_4$ tetrahedra with the B_{12} cluster *via* edge-sharing (Fig. 3a). Meanwhile, Se2 is responsible for connecting two $SiSe_4$ tetrahedral units (Fig. 3b), also through edge-sharing. This arrangement of Se atoms is essential for the formation of the 3D structure, as it facilitates the strong bonding between the different clusters and tetrahedra resulting in the creation of tunnels within the framework. The sodium ions (Na^+) occupy these tunnels, residing within the spaces formed by the anionic framework. The charge balance of the compound is maintained by the oxidation states of the constituent elements: the $B_{12}Se_{12}$ cluster carries a charge of 14^-, silicon (Si) is in the +4-oxidation state, selenium (Se) in the 2^- state, and sodium (Na) in the +1 state. This charge balance ensures the overall stability of the compound, with the Na^+ ions playing a crucial role in charge compensation within the 3D network.

The sodium (Na) atoms in $Na_2B_{12}Si_6Se_{18}$ are coordinated with six neighboring selenium (Se) atoms, forming a $NaSe_6$ octahedral geometry (Fig. 3c). When these $NaSe_6$ polyhedra are extended throughout the three-dimensional structure, it becomes evident that the $NaSe_6$ units are interconnected *via* vertex-sharing (Fig. 3d). The Na–Se bond distance observed within the $NaSe_6$ octahedra is approximately 3.1813(5) Å, which is consistent with bond lengths reported for other compounds, such as $Na_4Si_2Se_{6-o}P_{48}$, $NaScSe_2$ and $NaCuTSe_3$.[32–34] The Si–Se bond distances vary slightly, ranging from 2.2777(9) Å to 2.2808(8) Å. These values are in close agreement with those observed in other selenium-containing silicate com-

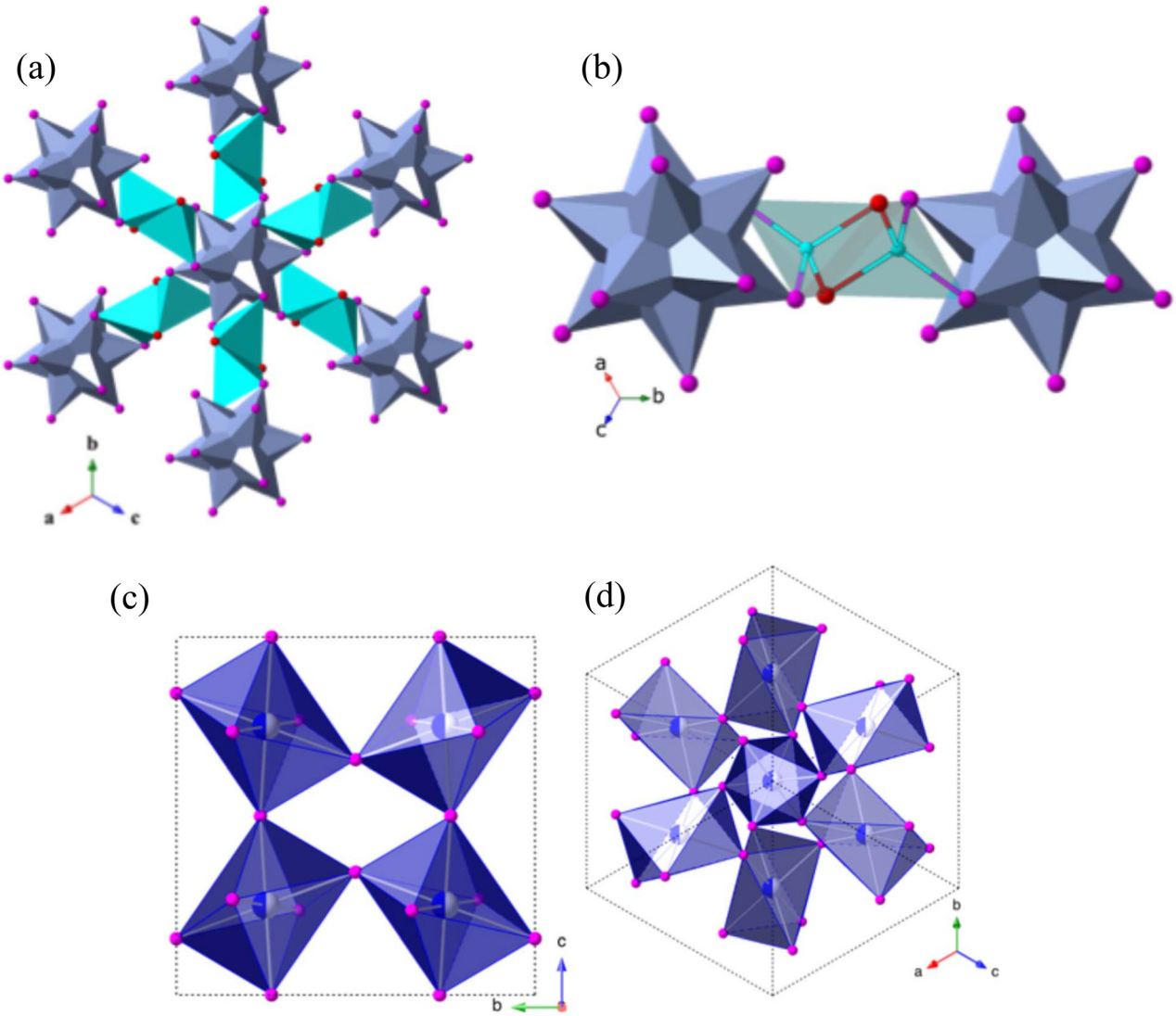

Fig. 3 The (a) polyhedral view of $[B_{12}Se_6]^{2-}$ icosahedron cluster extended along [111] direction, (b) bridging of $SiSe_4$ tetrahedra between two $[B_{12}Se_6]^{2-}$cluster, and (c and d) a representation of $NaSe_6$ octahedra and their connectivity with its neighboring $NaSe_6$ units.

pounds, including $Ba_6Si_{2-x}Ge_xSe_{12}$, Li_2HgMSe_4, $Na_2Hg_3M_2Se_8$, and Ba_3SiSe_5.[35–37] This consistency in Si–Se bond lengths across various compounds highlights the structural similarity and predictability of silicon–selenium bonding within tetrahedral frameworks. The B–Se bond length is approximately 1.980(3) Å, while the B–B distances range between 1.779(7) Å and 1.781(4) Å. These bond lengths are comparable to those found in related compounds, such as $CrSi_3(B_{12})Se_{12}$, $A_8[B_{12}(BSe_3)_6]$, and $Sn_{4-\delta}B_{12}Se_{12}[Q_x]$ (where Q = Se, Te), which also contain B_{12} icosahedral clusters.[9,21,31]

UV-visible diffuse reflectance spectroscopy

The optical properties of the quaternary $Na_2B_{12}Si_6Se_{18}$ polycrystalline compound was examined at room temperature through optical absorption studies. The absorption plot with respect to wavelength (nm) is shown in Fig. S7.† The Kubelka–Monk equation was employed to analyze the optical absorption data, as shown in Fig. 4. The band gap observed for the compound is ~2.1(1) eV, consistent with semiconducting behavior.

In situ powder X-ray diffraction (PXRD)

To better understand the formation of the $Na_2B_{12}Si_6Se_{18}$ phase and determine whether it forms during heating or cooling, we carried out a series of controlled thermal reactions. Initially, we heated a reaction mixture containing Na_2Se, Si, B, and Se (in a molar ratio of 1 : 6 : 12 : 17) to a temperature of 800 °C over a period of 4 hours. The sample was then held at this temperature for 36 hours, followed by quenching the red-hot reaction tube in ice-chilled water. To further investigate the effect of dwelling time and temperature on the phase formation, we repeated the thermal quenching experiment but

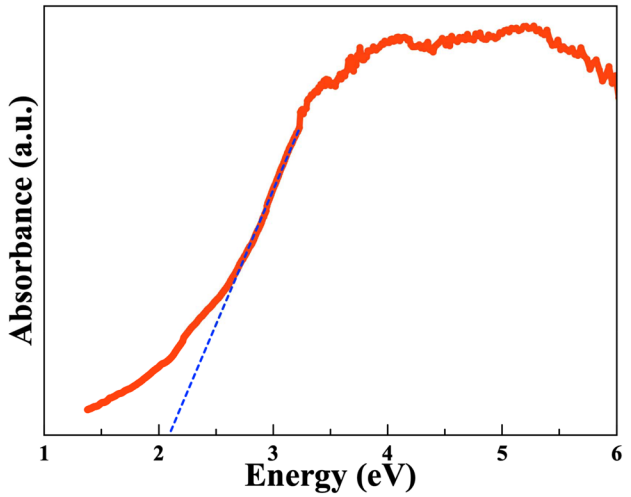

Fig. 4 The optical absorption plot of the polycrystalline $Na_2B_{12}Si_6Se_{18}$ compound.

reduced the dwelling time from 36 hours to 12 hours and lowered the reaction temperature from 800 °C to 600 °C. After these modified conditions, the samples were ground, and their powder X-ray diffraction (PXRD) patterns were collected for phase analysis. Our analysis revealed that the $Na_2B_{12}Si_6Se_{18}$ phase forms when the sample is heated to 800 °C, regardless of whether the dwell time is shorter or longer. However, no formation of the $Na_2B_{12}Si_6Se_{18}$ phase was observed when the sample was heated to temperatures below 800 °C (see Fig. S5†).

To gain a more detailed understanding of the phase formation process at different temperatures, we performed an *in situ* PXRD synthesis by loading the reaction mixture into a quartz capillary and heating the sample to 800 °C inside the hot stage of the X-ray diffractometer. This approach allowed us to monitor the phase evolution in real-time, providing insights into the specific conditions under which the $Na_2B_{12}Si_6Se_{18}$ phase forms Fig. 5.

The pattern for the initial reaction mixture contains peaks for Se_8, Si, and Na_2Se (the B used was amorphous), as expected. The first significant change in the patterns occurred between 200 and 250 °C: the peaks for Se and Na_2Se vanish leaving only the peaks for Si. This is most likely due to the Se_8 melting (M.P. = 221 °C) and dissolving the Na_2Se concurrently. The next major change occurs between 600 and 650 °C: the Si peaks disappear, and new peaks appear which do not correspond to the starting reagents or the final product. It is unclear what phase(s) these peaks belong to as the patterns could not be successfully matched to any known phases. Due to the simultaneous disappearance of the Si peaks, it is likely that this change is due to the reaction between the Si and the molten Se_8/Na_2Se mixture to form one or more selenosilicates. This may be enabled by either the solvation of the Si or the direct reaction requiring elevated temperatures. Finally, the last significant change in the pattern occurs between 700 and 750 °C: the peaks corresponding to the unknown phase(s) formed between 600 and 650 °C vanish and the peaks for the target phase, $Na_2Si_6B_{12}Se_{18}$, appear simultaneously. Due to the unknown identity of the peaks directly preceding those for $Na_2Si_6B_{12}Se_{18}$, it is unclear what phases are reacting to form the final product. However, it is clear that there is a minimum temperature (~750 °C) above which this reaction must be heated in order for the desired product to form.

Upon cooling, Fig. 6, only one significant change is observed: peaks for $Na_4Si_4Se_{10}$ appear at approximately 550 °C. This is a previously reported phase[38] consisting of Si_4Se_{10} super-tetrahedra separated by Na cations. The formation of this phase suggests that the B in the reaction mixture is completely consumed in the formation of the target phase, $Na_2Si_6B_{12}Se_{18}$, while the Na, Si, and Se are not.

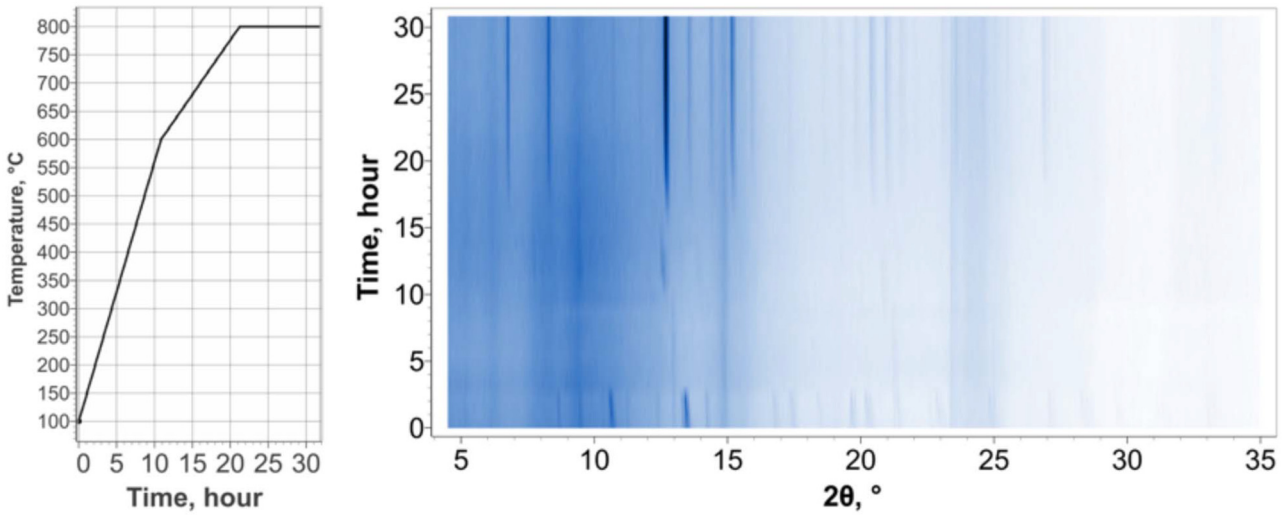

Fig. 5 The waterfall plot of the *in situ* PXRD patterns collected upon heating and annealing the reaction mixture. The waterfall plot is shown on the right as time *vs.* 2θ with the graph of temperature *vs.* time on the left.

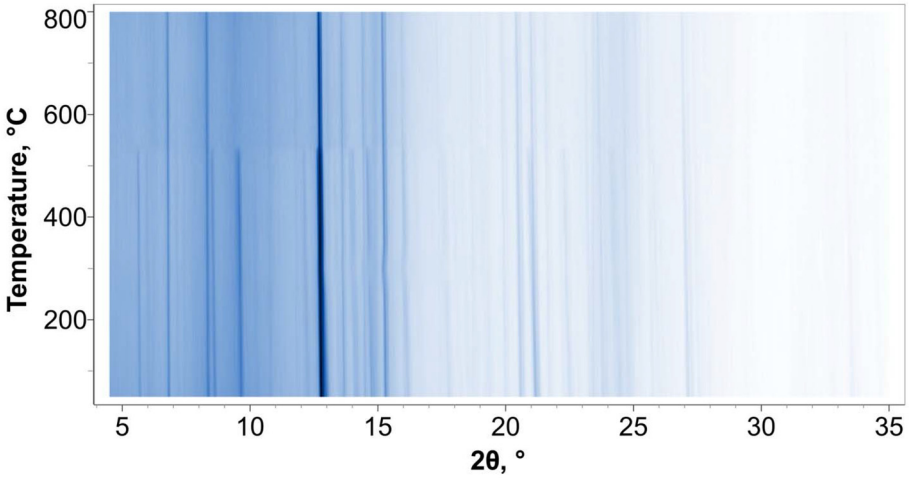

Fig. 6 The waterfall plot of the *in situ* PXRD patterns collected upon cooling the reaction mixture. The waterfall plot is shown as temperature *vs.* 2θ.

TGA studies

The thermal stability of $Na_2B_{12}Si_6Se_{18}$ polycrystalline powder samples was assessed using thermogravimetric analysis (TGA) (Fig. S6†). The TGA measurements were conducted under nitrogen flow, with the temperature increased at a rate of 5 °C min^{-1} to 500 °C. The results showed no significant weight loss, indicating the material's thermal stability under these conditions. To further confirm this, post-TGA powder X-ray diffraction (PXRD) analyses were performed on the samples. The PXRD patterns of the samples collected after heating revealed no structural degradation, confirming that the $Na_2B_{12}Si_6Se_{18}$ phases remained stable up to at least 500 °C, with no detectable phase transitions or decomposition occurring within this temperature range. As the material is synthesized above 800 °C, this is not unexpected.

Conclusion

The successful synthesis of the quaternary 3D chalcogenide compound $Na_2Si_6B_{12}Se_{18}$ *via* solid-state methods has revealed a distinctive framework featuring the rare icosahedral $[B_{12}]^{10+}$ cation. The assembly of this cation into a 3D tunnel structure filled with Na^+ ions, and its crystallization in the cubic $Im\bar{3}$ space group, highlight its complex and novel architecture. The structural connectivity between B_{12} icosahedra and $SiSe_4$ tetrahedra underscores the intricacy of the framework, while the compound's semiconducting properties, with a bandgap of 2.1 (1) eV, point to potential applications in electronic materials. The *in situ* PXRD studies further emphasize the phase formation process at different temperatures. The thermal stability of the material was confirmed by TGA/DSC measurements.

Data availability

The CCDC 2362801† entries encompass the supplementary crystallographic data associated with this paper. Raw data for other measurements are available upon request.

Conflicts of interest

The authors declare no competing financial interest.

Acknowledgements

The authors gratefully acknowledge the support from the U.S. Department of Energy, Office of Basic Energy Sciences, Division of Materials Sciences and Engineering, under award DE-SC0018739. Synthesis, structural characterization, optical, TGA, and *in situ* PXRD studies were conducted at the University of South Carolina.

References

1 R. B. King, *Chem. Rev.*, 2001, **101**, 1119–1152.
2 T. J. Udovic, M. Matsuo, A. Unemoto, N. Verdal, V. Stavila, A. V. Skripov, J. J. Rush, H. Takamura and S. Orimo, *Chem. Commun.*, 2014, **50**, 3750–3752.
3 M. P. Pitt, M. Paskevicius, D. H. Brown, D. A. Sheppard and C. E. Buckley, *J. Am. Chem. Soc.*, 2013, **135**, 6930–6941.
4 B. Krebs and H.-U. Hürter, *Angew. Chem., Int. Ed.*, 1980, **19**, 481–482.
5 B. Krebs, *Angew. Chem., Int. Ed.*, 1983, **22**, 113–134.
6 B. Krebs and W. Hamann, *J. Common Met.*, 1988, **137**, 143–154.
7 C. Jansen, J. Küper and B. Krebs, *Z. Anorg. Allg. Chem.*, 1995, **621**, 1322–1329.
8 A. Lindemann, J. Kuchinke and B. Krebs, *Z. Anorg. Allg. Chem.*, 1999, **625**, 1165–1171.
9 A. Hammerschmidt, M. Döch, S. Pütz and B. Krebs, *Z. Anorg. Allg. Chem.*, 2004, **630**, 2299–2303.
10 A. Hammerschmidt, A. Lindemann, M. Döch and B. Krebs, *Z. Anorg. Allg. Chem.*, 2003, **629**, 1249–1255.
11 J. Kuchinke, A. Hammerschmidt and B. Krebs, *Solid State Sci.*, 2003, **5**, 189–196.

12 A. Hammerschmidt, A. Lindemann, M. Döch, C. Köster and B. Krebs, *Z. Anorg. Allg. Chem.*, 2002, **628**, 1561–1567.
13 A. Lindemann, J. Küper, W. Hamann, J. Kuchinke, C. Köster and B. Krebs, *J. Solid State Chem.*, 2001, **157**, 206–212.
14 C. Püttmann, H. Diercks and B. Krebs, *Phosphorus, Sulfur Silicon Relat. Elem.*, 1992, **65**, 1–4.
15 R. Bertermann, W. Müller-Warmuth, C. Jansen, F. Hiltmann and B. Krebs, *Solid State Ionics*, 1999, **117**, 245–255.
16 L. S. Breton, G. Morrison, M. R. Lacroix, P. S. Halasyamani and H.-C. zur Loye, *Chem. Commun.*, 2022, **58**, 7992–7995.
17 Y.-Y. Li, B.-X. Li, G. Zhang, L.-J. Zhou, H. Lin, J.-N. Shen, C.-Y. Zhang, L. Chen and L.-M. Wu, *Inorg. Chem.*, 2015, **54**, 4761–4767.
18 S.-S. Han, W.-D. Yao, S.-X. Yu, Y. Sun, A. Gong and S.-P. Guo, *Inorg. Chem.*, 2021, **60**, 3375–3383.
19 Y. Huang, Y. Zhang, D. Chu, Z. Yang, G. Li and S. Pan, *Chem. Mater.*, 2023, **35**, 4556–4563.
20 K. Kaup, K. Bishop, A. Assoud, J. Liu and L. F. Nazar, *J. Am. Chem. Soc.*, 2021, **143**, 6952–6961.
21 M. Sugimori, H. Fukuoka, H. Imoto and T. Saito, *J. Organomet. Chem.*, 2000, **611**, 547–550.
22 S.-P. Guo, G.-C. Guo, M.-S. Wang, J.-P. Zou, H.-Y. Zeng, L.-Z. Cai and J.-S. Huang, *Chem. Commun.*, 2009, 4366–4368.
23 S.-H. Lin, J.-G. Mao, G.-C. Guo and J.-S. Huang, *J. Alloys Compd.*, 1997, **252**, L8–L11.
24 *APEX3 Version 2019.1-0 and SAINT+ Version 8.40A*, Bruker Nano, Inc., Madison, WI, USA, 2019.
25 SADABS-2016/2: L. Krause, R. Herbst-Irmer, G. M. Sheldrick and D. Stalke, *J. Appl. Crystallogr.*, 2015, **48**, 3–10.
26 (*a*) SHELXT: G. M. Sheldrick, *Acta Crystallogr., Sect. A: Found. Adv.*, 2015, **71**, 3–8; (*b*) SHELXL: G. M. Sheldrick, *Acta Crystallogr., Sect. C:Struct. Chem.*, 2015, **71**, 3–8.
27 C. B. Hübschle, G. M. Sheldrick and B. Dittrich, ShelXle: A Qt Graphical User Interface for SHELXL, *J. Appl. Crystallogr.*, 2011, **44**(6), 1281–1284.
28 P. Kubelka, *Z. Tech. Phys.*, 1931, **12**, 593–601.
29 S.-P. Guo, Y. Chi, B.-W. Liu and G.-C. Guo, *Dalton Trans.*, 2016, **45**, 10459–10465.
30 S.-S. Han, Q.-T. Xu, W. Liu and S.-P. Guo, *Dalton Trans.*, 2022, **51**, 4619–4622.
31 D. G. Chica, I. Spanopoulos, S. Hao, C. Wolverton and M. G. Kanatzidis, *Chem. Mater.*, 2021, **33**, 1723–1730.
32 F. Kamm, F. Pielnhofer, M. Schlosser and A. Pfitzner, *Inorg. Chem.*, 2023, **62**, 11064–11072.
33 G. Panigrahi, S. Yadav, S. Jana, A. Ghosh, M. K. Niranjan and J. Prakash, *New J. Chem.*, 2022, **46**, 22076–22087.
34 A. A. Berseneva, V. V. Klepov, K. Pal, K. Seeley, D. Koury, J. Schaeperkoetter, J. T. Wright, S. T. Misture, M. G. Kanatzidis, C. Wolverton, A. V. Gelis and H.-C. zur Loye, *J. Am. Chem. Soc.*, 2022, **144**, 13773–13786.
35 L. T. Menezes, A. Assoud and H. Kleinke, *Dalton Trans.*, 2023, **52**, 15831–15838.
36 L. Gao, J. Xu, X. Tian, B. Zhang, X. Wu and K. Wu, *Chem. Mater.*, 2022, **34**, 5991–5998.
37 H. Cheng, A. Tudi, P. Wang, K. Zhang, Z. Yang and S. Pan, *Dalton Trans.*, 2021, **50**, 11999–12005.
38 B. Eisenmann, J. Hansa and H. Schafer, *Z. Anorg. Allg. Chem.*, 1985, **40**, 450–457.